

AN ABSTRACT OF THE THESIS OF

Leah M. Bandstra for the degree of Master of Science in Oceanography presented on
May 13, 2004.

TITLE: High-Frequency Measurements of Total CO₂: Method Development and First Oceanographic Observations

Redacted for Privacy

Abstract approved: _____

Burke R. Hales

As concern grows about the long-term effects of increasing atmospheric CO₂ concentrations, it becomes increasingly important to understand the cycling of carbon on Earth, particularly in the dynamic marine reservoir. Gas exchange and relatively rapid ocean mixing times mean that the oceans play a significant role in determining the atmospheric CO₂ concentrations on annual and longer timescales. Over the last forty years, several large-scale projects have provided valuable marine carbon data, increasing the understanding of carbon cycling in ocean basin-scale processes. As more targeted projects are developed, traditional water column sampling techniques do not readily provide the high spatial resolution data necessary to understand small-scale processes. Towed instruments, such as the Lamont Pumping SeaSoar, have been developed which are capable of pumping a continuous sample stream to the shipboard laboratory for analysis. In order to maximize the amount of information obtained from the continuously flowing stream and achieve high spatial resolution, shipboard analyses must be performed at high temporal resolution.

This work describes the development of an analytical system to measure the total carbon dioxide (TCO₂) in a continuously flowing seawater stream at high

temporal resolution. The system uses a gas-permeable membrane contactor to extract the evolved CO_2 from an acidified stream and a non-dispersive infrared detector to analyze the CO_2 in the resulting gas stream. Laboratory tests have shown that the system responds with a time constant of 6 seconds and is able to resolve changes in signal with better than $\pm 0.1\%$ precision. Coulometric analyses of check samples collected in the field as well as analyses of internal check samples have shown the internal accuracy of the system to be reliable to $\pm 0.1\%$, and analyses of certified reference materials have shown the absolute accuracy to be better than $\pm 0.1\%$.

Coupled with the Lamont Pumping SeaSoar, the TCO_2 system has yielded high spatial resolution distributions of TCO_2 across the New England shelfbreak front. These TCO_2 data, in conjunction with collocated PCO_2 measurements of similar resolution, allowed us to calculate high spatial resolution distributions of alkalinity. Differences in distributions of alkalinity relative to TCO_2 shoreward and seaward of the front indicated a shift in phytoplankton assemblages as the front was crossed. Our measurements implicated biogenic calcium carbonate production on the seaward side of the front, as indicated by a near equivalence of TCO_2 and alkalinity depletion, and its absence shoreward of the front, as indicated by the absence of alkalinity depletion in areas of significant biological TCO_2 uptake. These high-resolution data can be coupled with collocated high-resolution physical data to calculate mixing and biological rates of production and calcite formation.

©Copyright by Leah M. Bandstra

May 13, 2004

All Rights Reserved

High-Frequency Measurements of Total CO₂:
Method Development and First Oceanographic Observations

by
Leah M. Bandstra

A THESIS

submitted to

Oregon State University

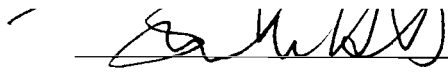
in partial fulfillment of
the requirements for the
degree of

Master of Science

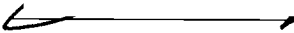
Presented May 13, 2004
Commencement June 2005

Master of Science thesis of Leah M. Bandstra presented on May 13, 2004.

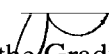
APPROVED: 
Redacted for Privacy


Major Professor, representing Oceanography

Redacted for Privacy

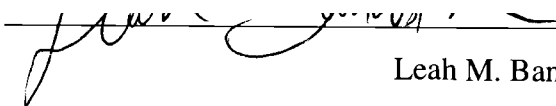

Dean of the College of Oceanic and Atmospheric Sciences

Redacted for Privacy


Dean of the Graduate School

I understand that my thesis will become part of the permanent collection of Oregon State University libraries. My signature below authorizes release of my thesis to any reader upon request.

Redacted for Privacy


Leah M. Bandstra, Author

ACKNOWLEDGEMENTS

I would like to thank Burke Hales for his friendship, guidance, and support over the course of this research. I have learned more from Burke than I thought possible, and I feel lucky to have had so many unique and valuable experiences as part of this group. After three years and seven cruises, I am looking forward to continuing my research with Burke.

I would also like to thank Dr. Taro Takahashi for his contributions to the development of this method and the analysis of our preliminary data. His analyses, advice, and insight allowed us to overcome many hurdles and roadblocks on the way to this point in this research.

I would like to thank crews of the R/V Thompson, R/V Endeavor, and R/V Revelle for some memorable cruises, where I learned a lot about the joys and pains of working at sea.

Joe Jennings deserves thanks for dealing with me in the lab, particularly on my very first cruise, and teaching me everything I ever wanted to know about performing chemical analyses at sea.

Thank you to my family and friends for the love and support that have helped me to get to this point. My family has provided me with so much throughout my life. I would not have gotten here without their invaluable guidance and perspective. My friends here in Corvallis and all of their amazing children have made this a wonderful place to live and have kept me going with their advice, love, and always generous contributions of food, drink, and hospitality.

Finally, I would not have had nearly as much fun getting here without Paul Covert and Dale Hubbard. In the lab, in class, at home, at sea, and in bars around the world, Paul and Dale have kept me sane, made me insane, and been two of the greatest friends I could ever hope to find.

CONTRIBUTIONS OF AUTHORS

Chapter II of this work benefited greatly from the contributions of Dr. Taro Takahashi of the Lamont-Doherty Earth Observatory of Columbia University. Dr. Takahashi's laboratory coulometrically analyzed discrete samples for TCO_2 concentrations, including samples collected at sea, internal check samples, standards, and certified reference materials, allowing for the verification of the internal and absolute accuracy of the analytical method described in this work. Dr. Takahashi also provided invaluable comments and insight during the development of the continuously flowing TCO_2 system.

TABLE OF CONTENTS

	<u>Page</u>
I. INTRODUCTION.....	1
II. DEVELOPMENT OF A SYSTEM FOR HIGH FREQUENCY TOTAL CO ₂ ANALYSIS.....	6
Abstract.....	7
1. Introduction and background.....	8
2. Objectives.....	11
3. Principle of method.....	11
4. Method description and operation.....	13
4.1 System description.....	13
4.2 Field calibration procedures.....	16
4.3 Laboratory calibration procedures.....	16
4.4 Discrete check samples.....	17
5. Results.....	17
5.1 Stripping efficiency.....	17
5.2 Response time.....	19
5.3 Stability and precision.....	19
5.4 Accuracy.....	23
6. Field results.....	23
7. Conclusion.....	33
III. CONCLUSION.....	35
BIBLIOGRAPHY.....	37
APPENDICES.....	41

LIST OF FIGURES

<u>Figure</u>	<u>Page</u>
1. Schematic of the TCO ₂ system.....	14
2. Stripping efficiency of TCO ₂ system.....	18
3. Response of TCO ₂ system.....	20
4. Stability and reproducibility of TCO ₂ system.....	21
5. Laboratory liquid calibration curve for TCO ₂ system.....	22
6. Time series of TCO ₂ data with discrete check samples.....	24
7. Map of study area showing cruise track for the data discussed.....	27
8. Gridded data for measured TCO ₂ , measured PCO ₂ , and calculated alkalinity transects across New England shelfbreak front.....	29
9. Alkalinity and TCO ₂ distributions.....	30

LIST OF APPENDICIES

<u>Appendix</u>	<u>Page</u>
Appendix A: Artificial seawater recipe and the carbon content of NaHCO_3 and salts.....	42
Appendix B: Membrane contactor stripping efficiency test.....	45
Appendix C Response time test and first-order model.....	46
Appendix D: Stability and precision of TCO_2 system.....	48
Appendix E: Accuracy check samples.....	49
Appendix F: Analyses of certified reference materials, Batch 63.....	50
Appendix G: Alkalinity calculations from TCO_2 and PCO_2	51

LIST OF APPENDIX TABLES

<u>Table</u>	<u>Page</u>
A1. Artificial seawater recipe.....	42
A2. Carbon content of cystine standards.....	42
A3. Carbon content of NaHCO_3 used to prepare standards for TCO_2 analyses.....	43
A4. Carbon content of salts used to prepare artificial seawater.....	44
B1. Data for range of $F_G:F_L$ and the associated stripping efficiencies.....	45
C1. XCO_2 change after step function change in input signal.....	46
C2. Model data fit to step function rise data	47
D1. Long-term stability of TCO_2 system.....	48
D2. Concentrations of TCO_2 standards (TCO_2) and LI-COR output (XCO_2).....	48
D3. Blank-corrected TCO_2 values and the deviations.....	48
D4. Independent check sample value.....	48
E1. Coulometrically-analyzed check samples.....	49
F1. Our analyses of CRM batch 63 samples.....	50
F2. LDEO analyses of CRM batch 63 samples.....	50

High-Frequency Measurements of Total CO₂: Method Development and First Oceanographic Observations

I. INTRODUCTION

The carbon cycle plays a major and essential role in Earth's biogeochemical processes. While deposits of fossil organic carbon and carbonate minerals contain the largest carbon reservoir on Earth, they cycle slowly in comparison to the ocean, atmosphere, and living biosphere and are often considered a long-term sink for carbon. The oceans contain 50 times more carbon than the atmosphere, and gas exchange allows the oceans to interact with the atmosphere on timescales of about a year. Because ocean mixing timescales are measured in years to centuries, the oceans play a significant role in determining atmospheric CO₂ concentrations on annual and much longer timescales.

Numerous studies over the last several decades have piqued interest in the connections between atmospheric and marine CO₂. Data obtained from the Vostok ice core (recently compiled in Petit et al., 1999) has shown large variability in atmospheric CO₂ concentrations over the last 420,000 years, ranging from 200 to 300 μatm over glacial/inter-glacial cycles. The cycles and variability seen in this data raise questions about the cause and effect relationships between natural land-based processes and atmospheric CO₂. In the last 50 years, work at Mauna Loa, Hawaii (as summarized in Keeling et al., 2004) has shown increases in atmospheric CO₂ since the onset of the industrial revolution, raising concern about the effects of anthropogenic activity on the atmosphere and climate. Martin (1990) proposed that connections existed between atmospheric CO₂ concentrations and the aridity of land, with increased aridity increasing the iron supply to the oceans, stimulating marine productivity and decreasing the atmospheric CO₂ concentrations. These data and hypotheses have led to the desire for the precise and accurate measurement of marine carbonate chemistry in order to better understand these connections between the atmosphere and the oceans and how anthropogenic activity might impact the carbon cycle.

When CO_2 dissolves in water, hydration occurs, forming carbonic acid, H_2CO_3 . Carbonic acid subsequently dissociates into bicarbonate (HCO_3^-) and carbonate (CO_3^{2-}) ions, releasing a hydrogen ion with each dissociation. The concentrations of these ions cannot be measured directly, but their concentrations can be calculated based on temperature- and pressure-dependent acid-base equilibrium relationships between the species. To constrain the carbonate system, two of the following parameters must be measured: total alkalinity, pH, TCO_2 , or PCO_2 .

Total alkalinity is often not well defined, but can be thought of as the acid-neutralizing capacity of an aqueous system. For our purposes, we will define alkalinity as the sum of the major ions contributing to this capacity.

total alkalinity = $[\text{HCO}_3^-] + 2[\text{CO}_3^{2-}] + [\text{B}(\text{OH})_4^-] + [\text{other acid-base reactive species}]$
 Acid-base reactive species, including phosphate, silicate, ammonia, and some organic acids, contribute as well, but the conjugate bases of carbonic and boric acid play the major role in terms of their concentrations in seawater.

The concentrations of the species of the carbonate system are defined by the thermodynamic equilibrium constants and the pH of the aqueous system. The pH is generally defined by the negative log of the hydrogen ion activity.

$$\text{pH} = -\log \{ \text{H}^+ \}$$

The relationship between the concentration of the hydrogen ion and the measured activity is complicated because of the complex seawater medium. The concentrations of HSO_4^- and HF ion pairs are often incorporated as part of the total hydrogen ion activity (Pilson, 1998). Depending on which of these species are included, different pH scales are used. This distinction must be clearly made in order to properly apply the acid-base dissociation constants to the equilibrium relationships.

The total carbon dioxide, TCO_2 , is simply defined as:

$$\text{TCO}_2 = [\text{HCO}_3^-] + [\text{CO}_3^{2-}] + [\text{CO}_2^*]$$

where CO_2^* is the sum of carbonic acid and aqueous dissolved CO_2 , the vast majority of which is present as aqueous CO_2 .

Finally, the PCO_2 of a sample is the partial pressure of CO_2 that exists in a small gaseous headspace at equilibrium with a seawater sample. This is easily

calculated from the aqueous dissolved CO_2 and the Henry's law constant of CO_2 , which defines the solubility at a given temperature and pressure:

$$\text{PCO}_2 = [\text{CO}_{2(\text{aq})}]/K_{\text{H}}$$

This parameter is temperature, pressure, and salinity dependent, but these dependences are understood and have been empirically defined.

Measurement of any two of these four parameters, as well as temperature, pressure, and salinity, allows for the constraint of the carbonate system and the calculation of the other two parameters as well as the bicarbonate and carbonate ions. We have chosen to use TCO_2 and PCO_2 to constrain the carbonate system due to the unambiguous definitions of these two parameters and their direct connection to important parameters in carbon cycling processes. In addition, Hales, Chipman, and Takahashi (2004) successfully used a membrane contactor to measure PCO_2 continuously at high resolution. They attempted to measure TCO_2 using a similar system but were unsuccessful in obtaining the appropriate accuracy. We have modified their system in an effort to continuously measure TCO_2 at the appropriate precision and accuracy.

Large-scale projects, such as the World Ocean Circulation Experiment (WOCE), the Joint Global Ocean Flux Study (JGOFS), and the Ocean Atmosphere Carbon Exchange Study (OACES) global surveys in the 1990s, as well as the Transient Tracers in the Ocean (TTO) project in the 1980s, and the Geochemical Ocean Section Study (GEOSECS) in the 1970s, have made available a variety of high-quality marine organic and inorganic carbon data from around the world. While these large-scale projects provide invaluable data regarding the ocean basin-scale biogeochemical cycling of carbon, smaller projects with more targeted study areas are also important in understanding processes affecting marine carbon.

High spatial resolution measurements of the chemical properties of the water obtained with a pumping towed vehicle can provide more complete water column data than traditional sampling techniques, such as the Niskin bottle rosette-style sampler. The Lamont Pumping SeaSoar (Hales and Takahashi, 2002) is equipped with a pump, which continuously returns water to the shipboard laboratory through a tube in its tow

cable. This instrument undulates in the water column and can be towed behind a research vessel at about 6-7 knots. The Supersucker (Hales, in prep) consists of a sled-like platform that is towed from the side of a ship at about 2 knots while pumping water to the lab through a similar tow cable. Both instruments can be equipped with an array of *in situ* msensors, including a CTD, fluorometer, transmissometer, and oxygen sensor.

Because the SeaSoar and the Supersucker sample continuously, the shipboard analytical measurements must be made at high temporal resolution to obtain the desired spatial resolution. Such resolution has been accomplished for a suite of nutrients (Hales and Takahashi, 2004), PCO_2 (Hales, Chipman, and Takahashi, 2004), and now TCO_2 , as discussed in this work. These high-resolution chemical measurements, coupled with co-located high-resolution physical measurements, can provide the necessary data to specifically calculate parameters that could only be estimated by previous methods, including turbulent mixing-supported chemical fluxes and biological uptake rates of nutrients and carbon species. Data of this kind will further the understanding of biogeochemical cycles in the oceans.

There are several challenges associated with high temporal resolution analyses using these methods. As the seawater stream travels through the tow cable, the stream mixes to a certain extent, and some of the high frequency variability and fine structure in the sample stream can be lost. To minimize this effect and preserve as much detail as possible from the sample stream, it is important to minimize the response times of the shipboard analytical systems. In addition, it is important to analyze the sample stream continuously to retain the fine detail, as subsampling with discrete samples would lead to a loss of data between samples.

This work describes the theory and operation of an analytical system developed to accurately and precisely measure the TCO_2 concentration of a continuously-flowing seawater stream at high resolution. Preliminary data collected at the New England shelfbreak front in summer 2002 using the Lamont Pumping SeaSoar are also presented as proof-of-concept of the technique, along with the first-

of-their kind high-resolution observations of measured TCO_2 and calculated alkalinity, which allow distinction of calcitic and non-calcitic phytoplankton communities.

II. DEVELOPMENT OF A SYSTEM FOR HIGH FREQUENCY TOTAL CO₂ ANALYSIS

A manuscript by Leah Bandstra, Burke Hales, and Taro Takahashi
to be submitted to Marine Chemistry.

ABSTRACT

We developed a system to accurately, precisely, and rapidly measure total inorganic carbon (TCO_2) in a continuously flowing seawater stream. The system is based on a gas-permeable membrane contactor, through which CO_2 evolved from an acidified seawater stream is continuously stripped by a flowing gas stream. The CO_2 content of this strip-gas stream, which is proportional to the TCO_2 of the seawater stream via a simple mass balance, is then analyzed using a non-dispersive infra-red (NDIR) gas analyzer. Laboratory results have shown that the system has a response time of 6 seconds and is able to resolve changes in signal with better than $\pm 0.1\%$ precision. Independent coulometric analyses of check samples collected in the field, analyses of internal check samples, and analyses of certified reference materials have shown the accuracy of the system to be reliable to $\pm 0.1\%$.

Coupled with the Lamont Pumping SeaSoar system, the TCO_2 system has yielded high spatial resolution distributions of TCO_2 across the New England shelfbreak front. These TCO_2 data, in conjunction with collocated PCO_2 measurements of similar resolution, allowed us to calculate high spatial resolution distributions of alkalinity. Distributions of alkalinity relative to TCO_2 , in the context of nitrate and silicate uptake rates and *in situ* measurements of optical backscatter and fluorescence, indicated that biogenic calcium carbonate production plays an important role in offshore waters and in surface waters across the New England shelfbreak front.

1. Introduction and background

The ocean is the largest dynamic reservoir of carbon on Earth, storing about fifty times more carbon than contained in the atmosphere. Air-sea exchange and century-scale ocean mixing times mean this large reservoir must have a dominant influence on atmospheric CO_2 over these timescales. The precise and accurate constraint of the marine carbonate system can help answer questions regarding the affects of anthropogenic CO_2 increases on the global carbon cycle. In addition, photosynthesis and respiration and biogenic calcite formation and dissolution directly affect the marine inorganic carbon pool by uptake and release of CO_2 and carbonate, respectively. These biological processes can be better understood through the careful study of the marine carbonate system.

Upon dissolution in the ocean, carbon dioxide forms carbonic acid, which dissociates to bicarbonate, carbonate, and hydrogen ions, which have a controlling role in the acid-base chemistry of the world's oceans. The concentrations of the bicarbonate and carbonate ions cannot be measured directly, but their concentrations can be calculated based on other measurable quantities and thermodynamic relationships, which are functions of the temperature, pressure, and salinity of the seawater. With these physical properties known, the system can be constrained simply by measuring two of the parameters of the carbonate system (described in numerous publications; early summary in Park, 1969; recent discussion in Millero, 1995).

The measurable parameters of the carbonate system include total alkalinity (TA), pH, total inorganic carbon (TCO_2), and the partial pressure of CO_2 (PCO_2). Total alkalinity is defined as the sum of the normalities of acid-base reactive anions minus the sum of normalities of the acid-base reactive cations, while pH is proportional to the log of the hydrogen ion activity or concentration, depending on scale conventions. Total inorganic carbon is the sum of the concentrations of bicarbonate ion, carbonate ion, and aqueous CO_2 . Finally, PCO_2 is the CO_2 pressure that exists at equilibrium in a small gaseous headspace above a seawater sample.

All four quantities have been measured in the field at appropriately high precision to constrain the carbonate system, but the total alkalinity and pH

measurements suffer when high accuracy is required. The complex seawater medium has led to different scale conventions for the pH measurement, as the variable ionic strength of seawater affects the activity coefficient of the hydrogen ion and the electrodes used for potentiometric measurements of pH (Pytkowicz, 1966; Dickson, 1984, 1993a, 1993b). Recently, alkalinity measurements made during the World Ocean Circulation Experiment/Joint Global Ocean Flux Study/Ocean Atmosphere Carbon Exchange Study (WOCE/JGOFS/OACES) cruises have been shown to require large corrections for inaccuracies (Lamb et al., 2002), perhaps due to inaccuracies in the conceptual models of which ionic species contribute to the alkalinity balance. As a result, we chose not to consider measurement of these parameters in our quest to constrain the carbonate system, focusing instead on PCO_2 and TCO_2 .

PCO_2 has been measured with appropriate precision and accuracy at high resolution by equilibrating a carrier gas with a continuously-flowing seawater stream using showerhead-style equilibrators (Broecker and Takahashi, 1966) and with gas permeable membrane contactors (Hales, Chipman, and Takahashi, 2004). In both the showerhead- and contactor-based systems, the CO_2 in the equilibrated gas stream is quantified using non-dispersive infra-red (NDIR) analysis. Hales, Chipman, and Takahashi (2004) were able to continuously measure the PCO_2 of a continuously flowing seawater sample with state-of-the-art precision and accuracy with response times of seconds. This approach provides a constraint on carbonate chemistry at the high sampling frequencies we desire.

TCO_2 measurement has evolved over the last several decades, but the generally used state-of-the-art methods involve acidification of a seawater sample and quantitative measurement of the evolved CO_2 . Originally, the evolved CO_2 was measured either by gas chromatography (Park, 1964; Weiss and Craig, 1973) or infra-red absorption (Broecker and Takahashi, 1966; Wong, 1970), with gas chromatography generally preferred for fieldwork due, in part, to at-sea calibration complications (Kanomori, 1982). Dyrssen and Sillen (1967) developed the potentiometric titration method for measuring the evolved CO_2 , although the appropriate accuracy and precision for measuring CO_2 invasion could not be achieved

with this method. Coulometric analysis (Johnson, 1985, 1987, 1993) is now the accepted procedure for the accurate measurement of the TCO_2 of a seawater sample and is used on major oceanic survey programs (Dickson and Goyet, 1994).

Coulometry involves the titration of the seawater sample with electro-generated OH^- ions to a neutral endpoint, which is detected photometrically (Johnson, 1985). This measurement achieves the high precision and accuracy necessary for the TCO_2 measurement, however it involves unstable chemicals, hours of conditioning and start-up time, and 20 minutes or more per coulometric titration. The methods involving NDIR detection do not face these limitations, and technological improvements have led researchers to reexamine NDIR as a viable detection option for field studies.

Goyet and Snover (1993) compared a coulometric system to an NDIR detection system in the laboratory and found that the two methods gave comparable results in terms of reproducibility and accuracy. O'Sullivan and Millero (1998) performed TCO_2 measurements using NDIR detection in the field, subsampling from a surface seawater line and integrating under the infrared absorbance peak. They verified their values against a coulometric system also used in the field and found that the two systems gave similar results within the respective uncertainties. Kimoto et al. (2002) have also developed a subsampling TCO_2 analyzer using NDIR with time resolution of nearly one sample per minute, and their values agree with coulometer-obtained values to $\pm 0.24\%$, on average. While their sampling rates represent an improvement over those of traditional coulometric methods, the system developed by Kimoto et al. (2002) does not respond with the speed of the Hales, Chipman, and Takahashi (2004) PCO_2 system with which we are attempting to couple our TCO_2 system. In this paper, we present the theory and operation of the first ever continuous TCO_2 system, as well as the first high-resolution field measurements made using this instrument.

2. Objectives

Both the established PCO_2 system of Hales, Chipman, and Takahashi (2004) and the TCO_2 system described here have been developed to merge with continuously-sampling towed profiling vehicles, such as the Lamont Pumping SeaSoar (Hales and Takahashi, 2002) or the Supersucker (Hales, in prep), which pump seawater continuously to the ship-board lab through a tow cable with a tube in its core. Hales and Takahashi (2002) found that high-temporal frequency information in the sample stream is smeared during its travel through the cable with a time constant (e-folding time) of 7.5-10 seconds. Our goal was to develop a system for TCO_2 measurement with a time constant similar to that of the Hales, Chipman, and Takahashi (2004) PCO_2 measurement system, and less than the 7.5 seconds associated with smearing in the sampling tube.

Many processes of interest, including evasion of CO_2 from the atmosphere and biological processes, only change the TCO_2 by a few $\mu\text{mol/kg}$ out of the background TCO_2 concentrations around 2000 $\mu\text{mol/kg}$. The precision of the TCO_2 measurement must be $\pm 0.1\%$ or better to resolve these small changes in the large background signal. The absolute accuracy of the measurement is also important. We wish to use both the PCO_2 and TCO_2 measurements to calculate the speciation of the carbonate system without propagation of analytical uncertainties. We also wish to compare our data to historical marine carbonate system measurements obtained by coulometry, so our measurement must have at least the same accuracy as this state-of-the-art discrete method, which is accurate to about $\pm 0.1\%$ (Johnson, 1985).

3. Principle of method

Our system depends on the rapid and continuous stripping of CO_2 from an acidified seawater stream with a CO_2 -free strip gas, followed by continuous quantification of the CO_2 in the strip gas. This system uses a gas-permeable hydrophobic membrane contactor for the stripping, precisely controlled liquid sample and strip gas flows through the contactor, and continuous detection of the stripped CO_2 by non-dispersive infrared (NDIR) absorbance.

The gas-permeable membrane contactor used to measure TCO_2 is commercially available from Liqui-Cel (www.liquicel.com, #G477,) and consists of an array of hydrophobic microporous tubes housed in a polycarbonate casing. The tubes have an inner diameter of 250-300 μm , with 50 μm -thick walls and pores of about 0.3 μm in diameter. The acidified seawater sample stream passes through the inside of these tubes, and the evolved CO_2 diffuses through the pores, across the membrane, and into the gas stream, which flows countercurrent around the outside of the tubes.

On timescales corresponding to the gas and liquid flushing times of the contactor, a simple mass balance is achieved:

$$F_{L,in} \text{TCO}_{2,in} + \gamma F_{G,in} \text{XCO}_{2,in} = F_{L,out} \text{TCO}_{2,out} + \gamma F_{G,out} \text{XCO}_{2,out} \quad \text{Equation 1}$$

where $F_{L,in}$ and $F_{L,out}$ are the liquid flow rates in and out of the contactor, and $F_{G,in}$ and $F_{G,out}$ are the gas flow rates in and out of the contactor. $\text{TCO}_{2,in}$ and $\text{TCO}_{2,out}$ represent the TCO_2 concentration in the liquid stream at the inlet and outlet of the contactor, respectively. Finally, $\text{XCO}_{2,in}$ and $\text{XCO}_{2,out}$ represent the mole fraction of CO_2 in the gas stream, and γ is a conversion factor used to convert from mole fraction to volume of gas at STP. The inlet and outlet flows can be assumed to be equivalent, and the inlet gas is CO_2 -free, so Equation 1 reduces to:

$$F_L \text{TCO}_{2,in} = F_L \text{TCO}_{2,out} + \gamma F_G \text{XCO}_{2,out} \quad \text{Equation 2}$$

We can define the efficiency, E , as the fraction of the TCO_2 entering in the liquid stream which is stripped from the seawater sample:

$$E = \frac{F_L \text{TCO}_{2,in} - F_L \text{TCO}_{2,out}}{F_L \text{TCO}_{2,in}} \quad \text{Equation 3}$$

Combining and rearranging Equations 2 and 3 gives an equation for the TCO_2 concentration of the seawater sample based on the stripping efficiency, the gas and liquid flow rates, and the mole fraction of CO_2 in the strip-gas stream:

$$\text{TCO}_{2,\text{in}} = \frac{F_G}{F_L} \frac{\gamma X \text{CO}_{2,\text{out}}}{E}.$$

Thus, if the efficiency is high and the gas and liquid flow rates are constant, the inlet TCO_2 in which we are interested is simply related to the outlet $X\text{CO}_2$ of the strip-gas stream, which we continuously quantify using a calibrated NDIR detector.

4. Method description and operation

4.1 System description

Figure 1 shows a basic schematic of our TCO_2 system. Fluorinated ethylene propylene (FEP) tubing was used in the system due to the low gas permeability of this material. The main seawater line was filtered through a 50 μm filter before the sample stream was drawn for TCO_2 analysis. A positive displacement pump (available from Fluid Metering, Inc., www.fmipump.com, #RH1CKC) was used to pump the liquid sample at 20 mL/min from either a continuously flowing seawater stream or a set of standards of known TCO_2 concentration, which are described in further detail below. The seawater line and the standard vessels were plumbed to a multi-port selection valve (available from Valco Instruments Company, Inc., www.valco.com, model C25) immediately upstream of the pump to allow for liquid standardization. Immediately downstream of the pump, 10% HCl was injected into the liquid stream at approximately 0.3 mL/min using a simple mixing tee and a pump. We used an Ismatec peristaltic pump, but any pump capable of delivering a continuous stream of acid at the appropriate flow rates should be acceptable. The sample then flowed through a coil of approximately 60 cm of 1/16" ID FEP to ensure complete mixing of the acid before the sample entered the membrane contactor.

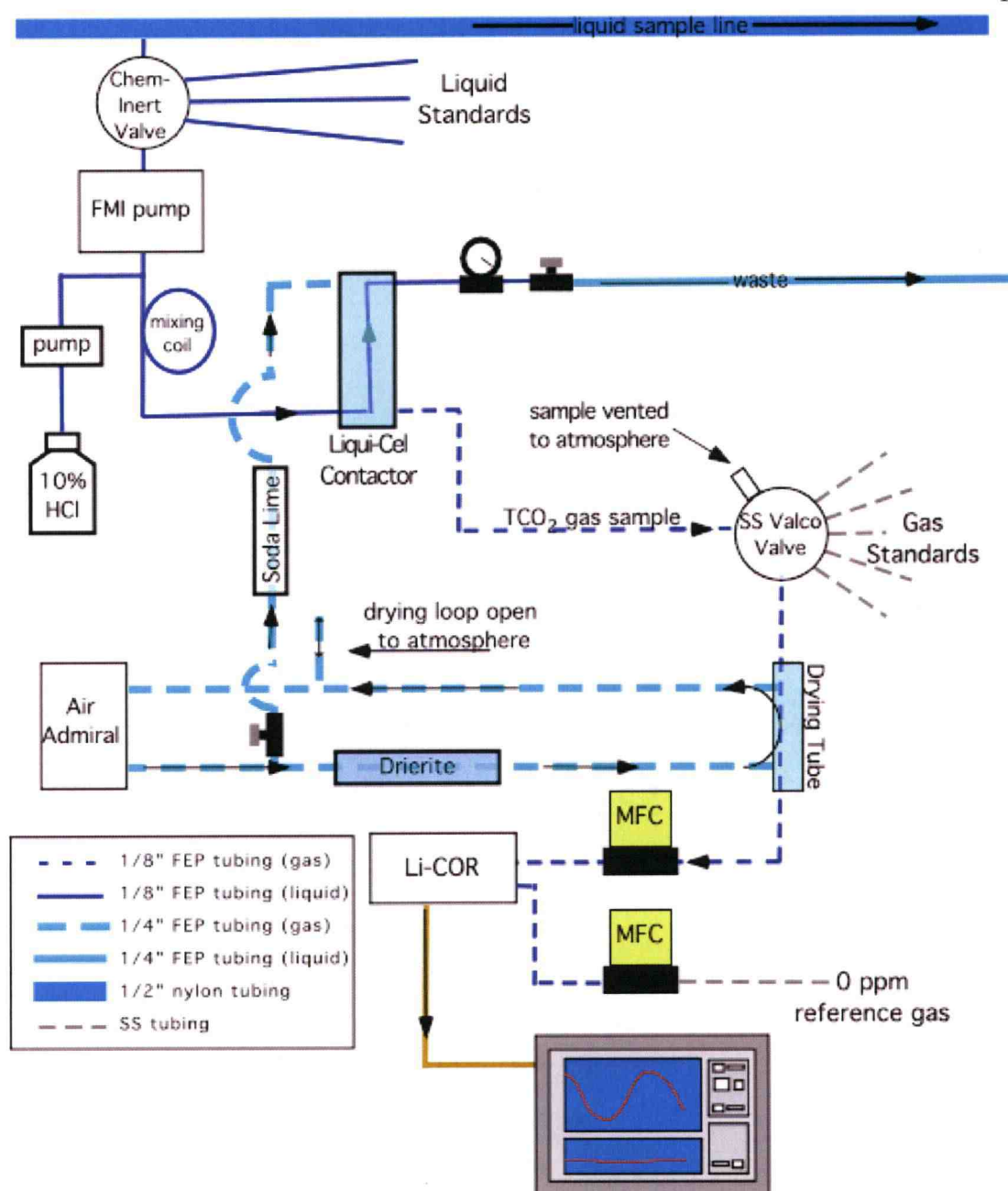


Figure 1. Schematic of the TCO₂ system. TCO₂ sample line is pumped from the main liquid sample line at 20 mL/min. Acidified sample stream flows through lumenside of contactor. Evolved CO₂ is stripped by counter-flowing CO₂-free gas stream on shellside. Strip gas stream is dried and CO₂ content is measured using NDIR detector. A mass flow controller controls the gas flow at 900 mL/min. Gas and liquid standards are used to calibrate signal.

The seawater was plumbed to the lumenside of the contactor (the inside of the tubes), and a continuously pumped gas stream flowed counter to the liquid on the shellside of the contactor (the outside of the tubes). The liquid sample stream exited the contactor and flowed to waste. A needle valve at the outlet of the lumenside was used to apply slight backpressure to the sample stream to prevent bubbles from catching in the contactor. A pressure gauge upstream of the needle valve allowed us to monitor the backpressure and keep it at a minimal positive pressure, ideally 0-2 psi.

The gas stream flowing through the membrane contactor was delivered using an Air Admiral vacuum/pressure pump (obtained from Cole-Parmer Instrument Company, www.coleparmer.com). To create the CO₂-free inlet gas, lab air was pumped through a column of soda lime to remove the CO₂ in the air before it entered the membrane contactor. Immediately downstream of the contactor, the gas stream entered a Perma-Pure drying tube (available from PermaPure, Inc., www.permapure.com, #MD-070-48P-2) consisting of a 48 cm length of Nafion tubing inside of a length of 1/8" ID tubing. In this dryer, the sample flowed through the Nafion as dry air flowed around it through the larger tubing, removing water vapor from the sample stream. Downstream of this dryer, the sample stream and a range of standard gases were plumbed to a stainless steel multi-port selection valve (available from Valco Instruments Company, Inc., www.valco.com, model SF) to allow for standardization of the NDIR gas analyzer. The outlet of the valve was plumbed to a mass flow controller (available from Aalborg, www.aalborg.com, #GFC-171), which maintained the gas flow through the system at 900 mL/min. Finally, the stream from the mass flow controller was plumbed to the sample inlet of the NDIR detector (available from LI-COR, Inc., www.licor.com, LI-COR 6262 CO₂/H₂O infrared gas analyzer). Ultrapure, CO₂-free air was used as a reference gas for the NDIR detector.

The system was managed using a PC, which collected data from the NDIR detector and controlled the standardization valves using software written in LabView. After collection, the data were synchronized with *in situ* CTD data, taking account of time lags associated with sampling and analysis times. The data were then gridded to a uniform 200 m horizontal by 0.5 m vertical grid, and grid points were filled with a

distance-weighted averaging scheme. The grid used is finer than the resolution of the data because of the variable horizontal spacing caused by the sawtooth pattern of the LPS.

4.2 Field calibration procedures

Our TCO_2 analysis system was designed to accommodate both gas and liquid calibration procedures. The standard gases used to calibrate the LI-COR were calibrated against Keeling manometric standards by gas chromatographic analyses at the Lamont-Doherty Earth Observatory (LDEO). In the field, we standardized the NDIR detector every two hours with sets of five of these gases. While the gas standard sequence was run, the sample gas stream was simply vented to the atmosphere to prevent overpressurization of the contactor.

At sea, sets of 3 liquid standards were prepared volumetrically using a 0.1 M NaHCO_3 stock solution and carbonate-free artificial seawater prepared using a recipe developed in our laboratory. In an attempt to minimize the exchange of atmospheric CO_2 with the standards, they were kept in glass bottles with plastic caps with holes. The sample tube was inserted through one hole in the cap and one was left open. These standards were also run every 2 hours in the field, with fresh standards prepared every 24 hours. While the liquid standard sequence was run, no seawater was pulled from the main sample line. To verify the absolute accuracy, these standards were subsampled as described in section 4.4 below and returned to the LDEO laboratory for coulometric analyses.

4.3 Laboratory calibration procedures

Gravimetric standards were prepared in the laboratory from a 0.1 M NaHCO_3 stock solution and carbonate-free artificial seawater. In general, 4 standards were prepared to establish the calibration curve, with an additional internal check sample prepared. This internal check sample was not included in the standard curve and was used to verify the internal accuracy of the TCO_2 system. While no carbonate species were added to the artificial seawater, it is possible that the salts used contained some

trace amounts of carbon, so the artificial seawater was run with the set of standards and used to blank-correct the final values. The carbon content of both the NaHCO_3 and the salts were verified by CHN analysis using a Carlo-Erba NA-1500.

4.4 Discrete check samples

Discrete samples collected at sea were used to test the accuracy of the flow-through system. The samples were collected from the outlet of the main sample line into sterilized 350 mL amber glass bottles with polyurethane-lined crimp-sealed metal caps. The bottles were rinsed several times with water from the flowing line, filled to within 5 mL of the top, and preserved with about 250 μL of saturated HgCl_2 solution before sealing. The standards were subsampled in a similar way, and the samples and standards were sent to LDEO for independent coulometric analysis and synchronized with the data obtained using the continuously flowing TCO_2 system.

5. Results

5.1 Stripping efficiency

The efficient stripping of CO_2 from the liquid stream is central to measuring TCO_2 using this system. We achieve sufficiently high efficiency with a gas flow of 900 mL/min and a liquid flow of 20 mL/min. Figure 2 shows the increasing efficiency as the ratio of gas to liquid flows ($F_G:F_L$) increases, with the point at 45 representing the $F_G:F_L$ at which we routinely operate this system. The fact that this point is on the plateau of the curve means that any slight fluctuations in gas or liquid flows will not significantly affect the stripping efficiency. While it is important to note that we are not stripping 100% of the TCO_2 out of the liquid stream, it is equally important that the efficiency does not change significantly in response to system operational variables. The liquid standardization process accounts for the fact that less than 100% of the CO_2 is stripped out of the liquid stream and allows us to quantitatively determine the TCO_2 of the liquid stream.

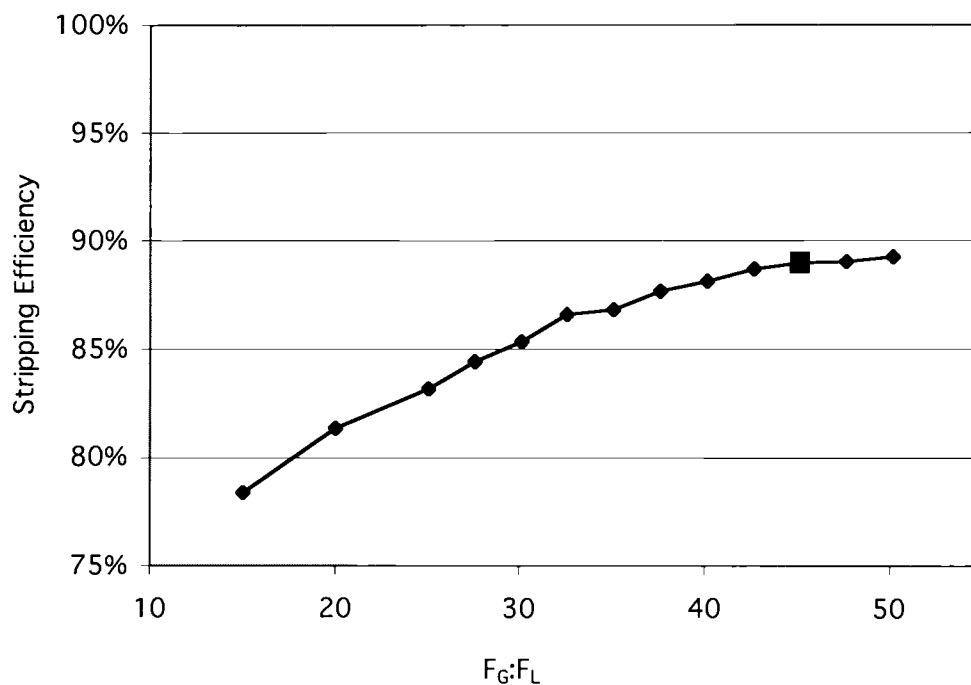


Figure 2. Stripping efficiency of TCO_2 system. Efficiency increases to a plateau as $F_G:F_L$ increases. Our system is run with a $F_G:F_L$ of 45, shown by square. Since this point is on the plateau, slight instrumental fluctuations in F_G or F_L will not significantly change the efficiency. This ratio reflects an appropriate balance between the stripping efficiency and the practical response time of the system.

5.2 Response time

In addition to affecting the stripping efficiency, the gas and liquid flows also dictate the response time of the system. Figure 3 shows the results of lab tests where a standard solution was pumped through the system, and a valve was used to switch to a solution of higher TCO₂ concentration. Use of the valve allows us to simulate a perfect step function change in input signal and then quantify how it is smeared due to travel through the TCO₂ system itself.

We modeled this curve with a simple first-order exponential rise (dashed line on Figure 3), as described by:

$$C(t) = C_o + (C_f - C_o)(1 - e^{-t/\tau})$$

where C_o is the initial value before the step function increase, C_f is the final value, and τ is the response time of the system. From this model, τ , also known as the e-folding time, was calculated to be 6 seconds.

This model accounts for smearing of the signal in the tube due to effects such as system memory, flow dead volumes, and backward mixing. While forward mixing also occurs in the tube and could be approximated with a more complicated smearing model, the simple first-order model fit the data sufficiently well to determine that the response time of the system was approximately 6 seconds.

5.3 Stability and precision

Figure 4 shows the results of long-term laboratory tests where a solution of known TCO₂ concentration was run on the system for several hours. The steps in signal shown at the beginning and end of the test represent sets of liquid standards, which were run to demonstrate that the signal returns to the same value after a drastic change in signal. These standard sets are reproducible to within $\pm 0.1\%$ at the beginning and end of the test. The average deviation of the signal from the mean is about $\pm 0.07\%$ over the 90 minutes in between standard curves, and there does not appear to be any long-term drift of the signal.

Figure 5 demonstrates the precision of the system with a typical laboratory liquid standard curve for the TCO₂ system, showing the gas-calibrated LI-COR signal

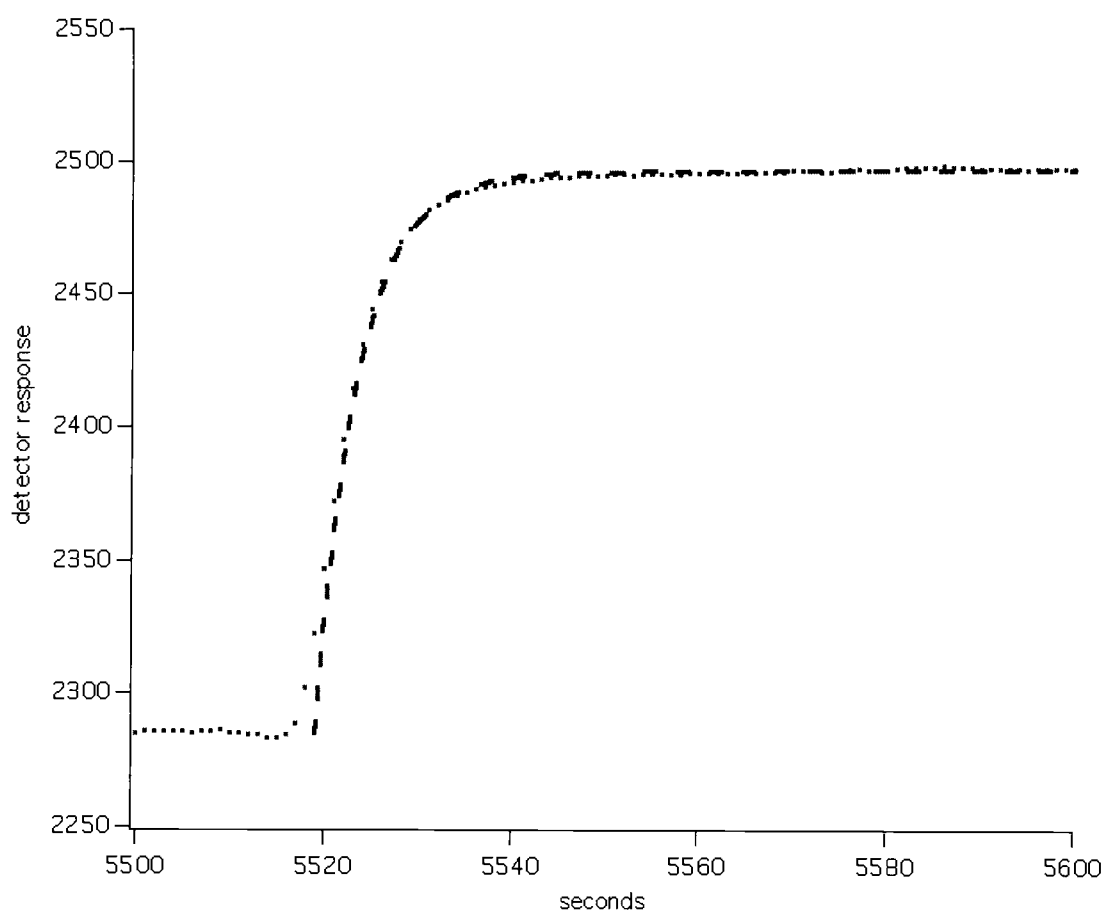


Figure 3. Response of TCO_2 system. Change in input was created using valve to prevent bubbles and maintain the step function, which is smeared by travel through the system, as shown by the dotted line. The simple first order exponential rise equation, discussed in section 5.2, was used to model the data and determine an e-folding time (τ) of 6 seconds.

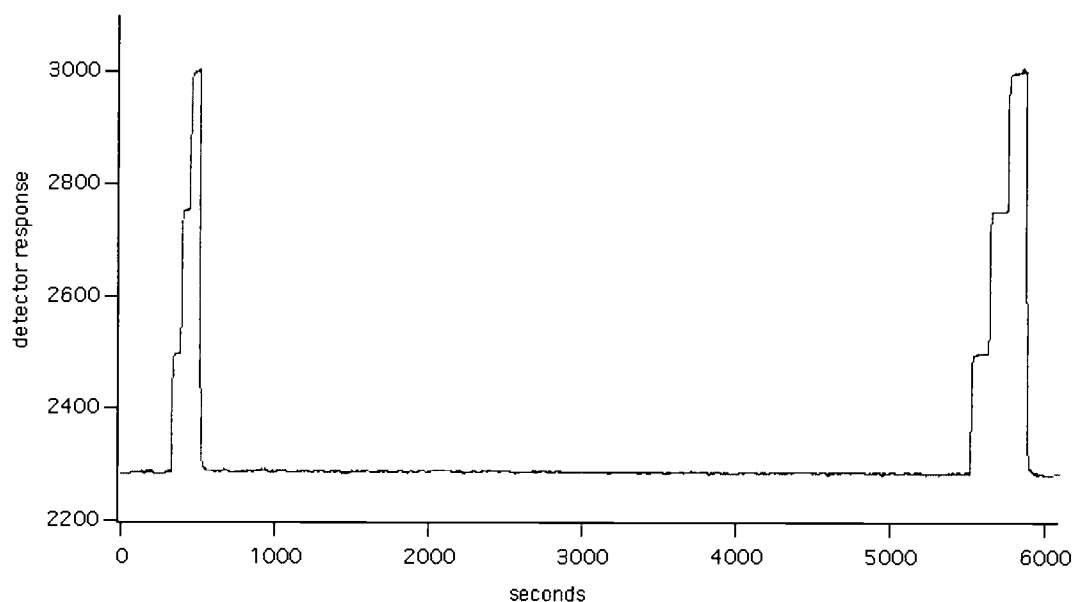


Figure 4. Stability and reproducibility of TCO_2 system. Detector response is proportional to TCO_2 . The signal, achieved by pumping a NaHCO_3 solution through the system, shows a deviation of 0.07% over about 90 minutes. No long-term drift is evident, the signal returns to the original value after standards are run, and each set of standards gives reproducible values to within 0.1% at the beginning and end of the test.

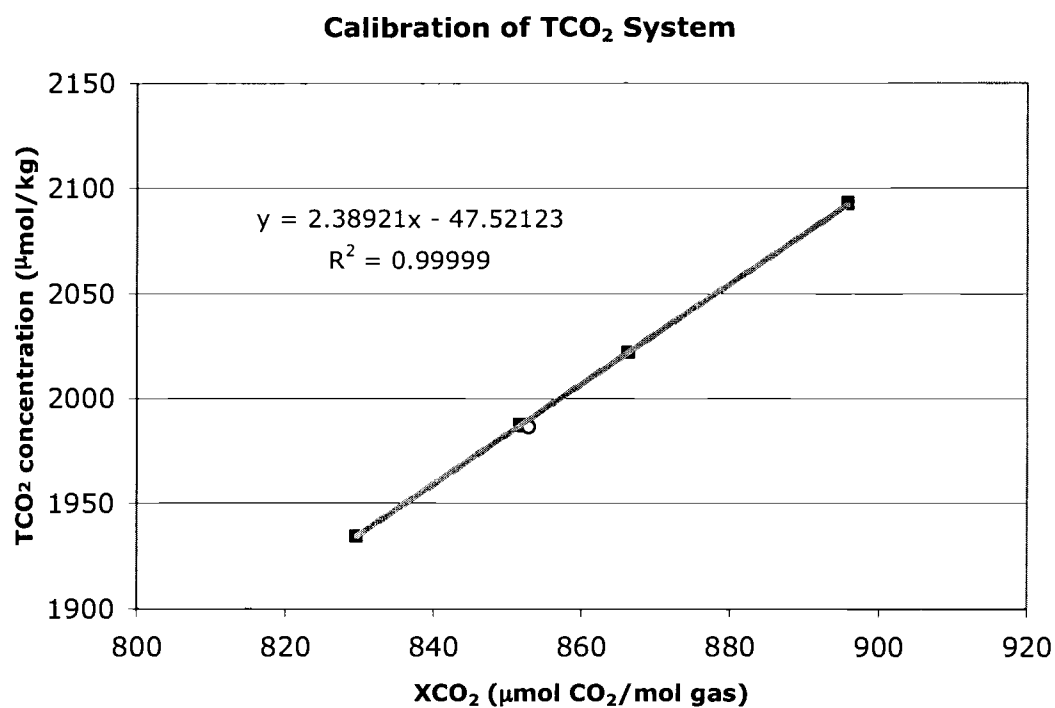


Figure 5. Laboratory liquid calibration curve for TCO₂ system. This plot shows mole fraction of CO₂ (XCO₂ obtained from NDIR detector) versus TCO₂ concentration of the prepared liquid standards. The average deviation from the linear regression shown is 0.009%. The internal check sample, represented by the open circle, is 0.15% from the line.

versus the concentration of the prepared liquid standard. The average deviation from the linear regression shown is $\pm 0.009\%$, with an R^2 of 0.99999. In addition, an internal check sample was also run at the time of this calibration curve. Based on the regression shown, the value of this sample was calculated to be within 0.15% of the prepared solution. On average, the internal check samples agreed with prepared value to within $\pm 0.1\%$.

5.4 Accuracy

Figure 6 shows a time-series of TCO_2 measured with the system described above in the sample stream of the Lamont Pumping SeaSoar (LPS) as it traveled through the water column during field operations in the vicinity of the New England shelfbreak front in August of 2002. High TCO_2 values in this series correspond to sample drawn while the LPS was at depth, and low TCO_2 values correspond to samples drawn while the LPS was in surface water. Open circles represent the TCO_2 content of the discrete check samples collected and analyzed coulometrically at LDEO. Average relative deviation between the discrete check samples and those measured by the continuously-flowing TCO_2 system described above was less than $\pm 0.08\%$.

Certified reference materials (CRMs) were also analyzed using the TCO_2 system, as summarized in Table 1. Our analyses agreed with the given values to within $\pm 0.11\%$. Additionally, the CRMs were analyzed coulometrically at LDEO, and our analyses agreed with these values to within $\pm 0.02\%$.

6. Field Results

This system was successfully used during four cruises: one in the Pacific sector of the Southern Ocean in January 2002, two at the New England shelfbreak front in Summer 2002, all using the Lamont Pumping SeaSoar (LPS, Hales and Takahashi, 2002) as the sampling device, and one off the Oregon coast in January 2003 using the Supersucker (Hales, in prep), a low-speed winch-controlled towed sampling vehicle

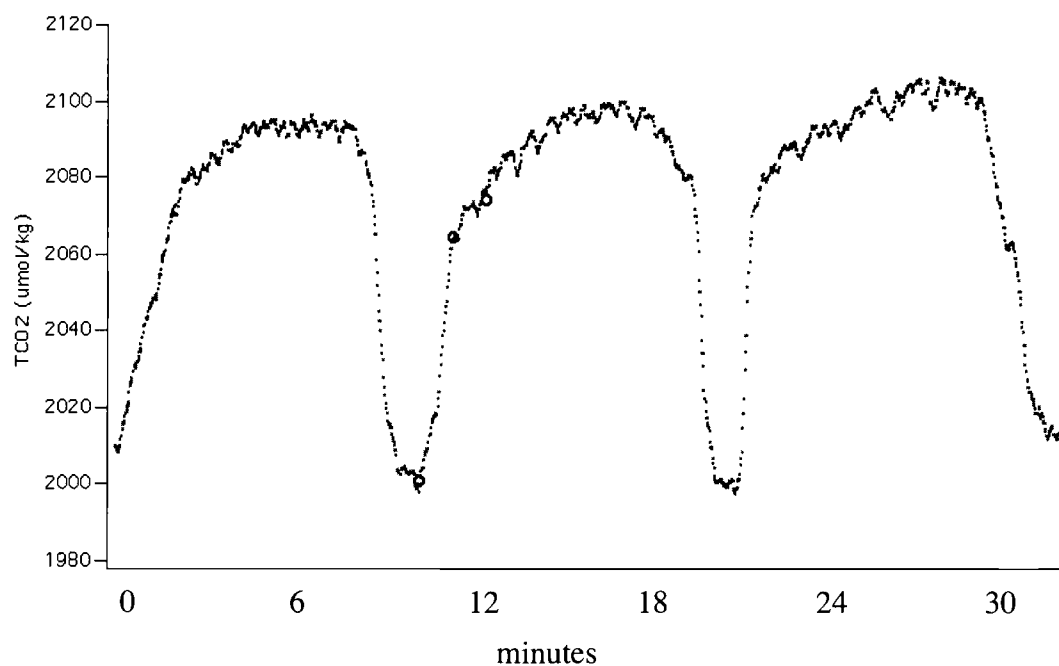


Figure 6. Time series of TCO₂ data with discrete check samples. Note the sawtooth path of the SeaSoar with time, showing high TCO₂ concentrations in deep water and lower concentrations in shallow water and a steep gradient. The open circles represent discrete check samples, which average a $\pm 0.08\%$ deviation from the TCO₂ system data.

Table 1. Analyses of certified reference materials. The numbers in parentheses indicate the total number of analyses and the number of separate bottles analyzed, respectively.

Source	[TCO ₂] $\mu\text{mol/kg}$
Certified value from SIO	2016.02 ± 0.47 (10, 10) ^a
LDEO	2014.1 ± 1.01 (6, 2) ^b
This work	2013.8 ± 2.06 (11,6)

^a These value were obtained manometrically at Scripps Institute of Oceanography, using methods described at <http://andrew.ucsd.edu/co2qc/methods.html>.

^b These values were obtained at LDEO coulometrically, using methods described in Johnson (1985, 1987, 1993).

for sampling. Here, we show and discuss preliminary data collected at the New England shelfbreak front at approximately 70.4°W and 40°N in August 2002. We performed several cross-front surveys from 39.95°N - 40.25°N at various longitudes, spanning the transition from shelf water to open ocean water several times at the high spatial resolution inherent to the LPS, in this case at about 1 km in the horizontal. The following discussion focuses on one survey on August 11, 2002 that consisted of three N-S sections across the front (Figure 7). Because of the orientation of the shelf-break isobaths, the southern extensions of the transects are offshore, and the northern extensions onshore, of the front. The front is located at about 40.05°N , corresponding to the repeated deviations from the straight north-south lines seen in the cruise track where the ship maneuvered around the fishing gear consistently deployed there.

Figure 8A shows the first-of-their-kind cross-front distributions of TCO_2 measured using the system described above. The locations of actual measurements made along the LPS track are overlain on the gridded data to demonstrate the density of the data used to create these sections. The highest TCO_2 concentrations are seen deep and offshore of the front, while deep onshore waters show lower concentrations. The front is a complicated transitional region, and surface water concentrations are consistently lower than deepwater concentrations across the front.

PCO_2 data were collected using a system similar to that described in Hales, Chipman, and Takahashi (2004), and the gridded cross-shelf distributions are shown in Figure 8B. Like TCO_2 , PCO_2 shows low surface values and a complicated frontal transition. Unlike TCO_2 , deepwater PCO_2 concentrations are higher onshore than offshore.

For each pair of TCO_2 and PCO_2 measurements, we calculated alkalinity using a simple 'pseudo-alkalinity' model consisting of carbonate, bicarbonate, and borate ions and their acid-base equilibrium reactions. The gridded cross-front alkalinity distributions (Figure 8C) show high alkalinity deep water offshore and lower alkalinity deep water onshore of the front, consistent with the opposite cross-shelf trends in deep water PCO_2 and TCO_2 .

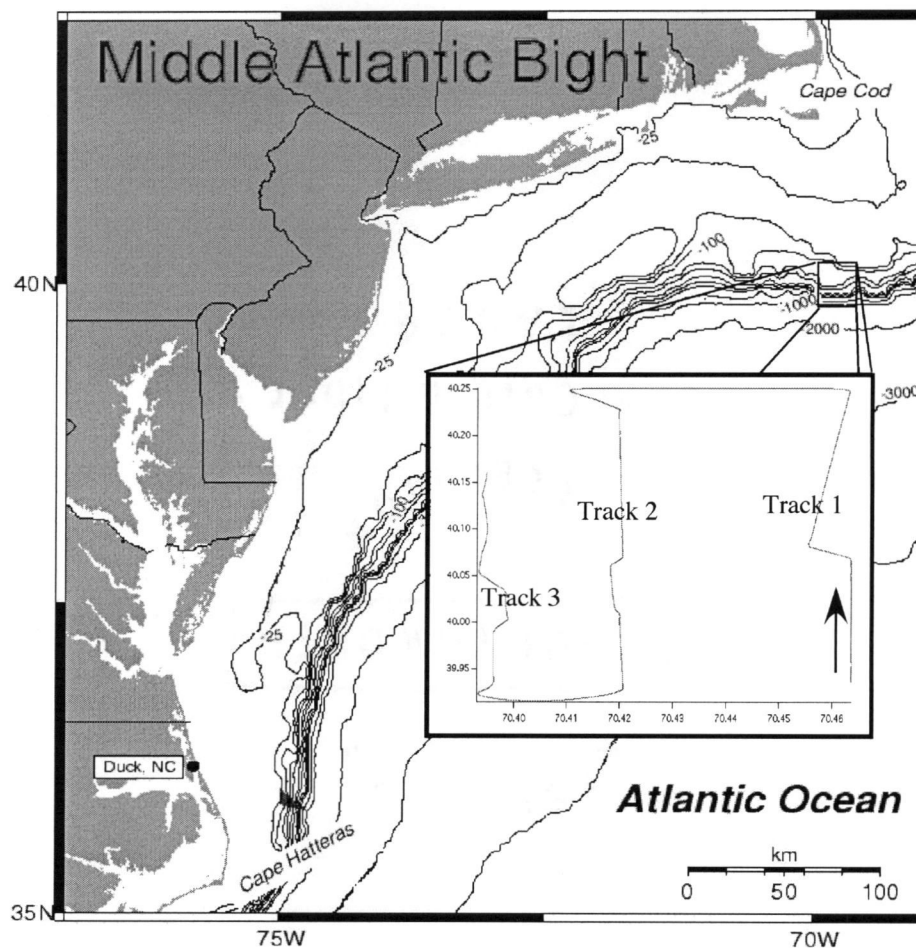


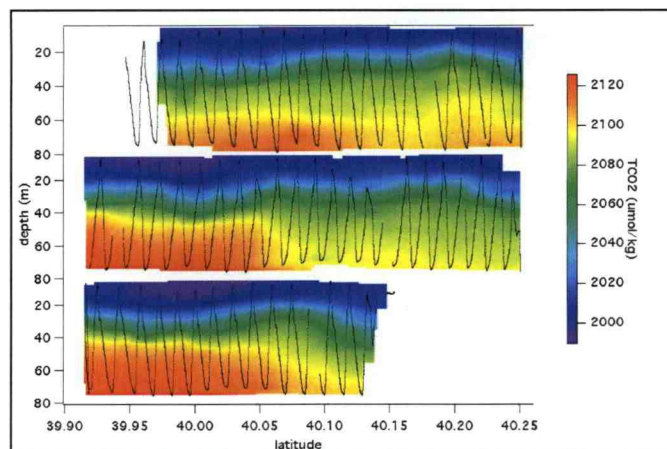
Figure 7. Map of study area showing cruise track for the data discussed. The small square indicates the approximate study area, and the blown up section shows the cruise track for the data discussed. The arrow indicates where the track begins, and the front exists at about 40.05 N. Offshore waters are south of the front, and onshore waters are north of the front.

These distributions can be better understood by examining the relationship between the changes in TCO_2 and alkalinity. Figure 9A shows TCO_2 versus alkalinity for the composite data shown in Figure 8; the colors represent the depth at which each measurement was taken. This depth distribution clearly shows that conservative mixing of deep offshore (point A) and onshore (point B) waters dominates the subsurface variability. Surface distributions are more complicated and are represented by departures from the deep conservative mixing line beginning at points C and D. These departures follow different paths before converging in surface waters, represented by points E and F.

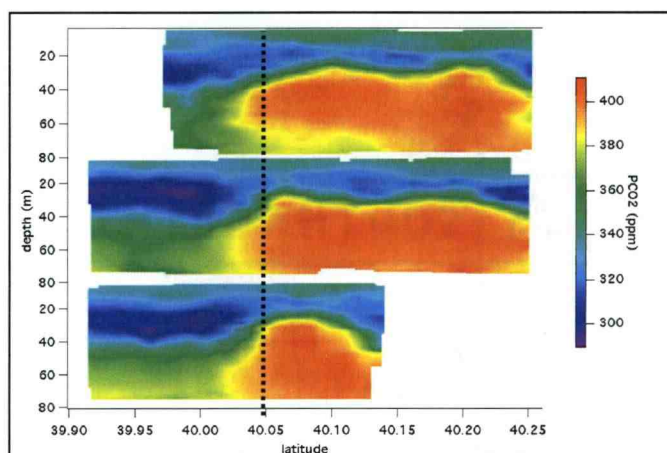
Two broadly-defined biological reactions can affect these distributions. Production and degradation of organic matter alone will affect the TCO_2 and alkalinity at a 7 to -1 ratio. If net production is occurring, the TCO_2 will decrease by seven units for every one unit increase in alkalinity. If respiration dominates, the TCO_2 will increase dramatically, and the alkalinity will decrease slightly. Calcite production and dissolution will have much different effects on TCO_2 and alkalinity. Biogenic calcite production will decrease the alkalinity 2 units for every one unit decrease in TCO_2 . Calcite dissolution will increase the alkalinity and TCO_2 at a ratio of 2 to 1. These processes are represented by the organic matter (OM) and calcite (C) arrows in Figure 9B.

The symbols in Figure 9B are color-shaded according to the latitude where the samples were collected. The coincidence of the OM arrow and the trend in the data onshore of the front implies that organic matter production dominates there, as TCO_2 is depleted from deep water concentrations but the alkalinity does not change significantly (from point D to F). In offshore samples, the alkalinity and TCO_2 both change, but alkalinity and TCO_2 change at a ratio of about 1 to 3 (from point C to E), implying that both organic matter and calcite production are responsible for the alkalinity and TCO_2 distributions in offshore waters. In the shallowest waters on either side of the front, the alkalinity and TCO_2 change at a ratio of about 1.5 to 1,

A)



B)



C)

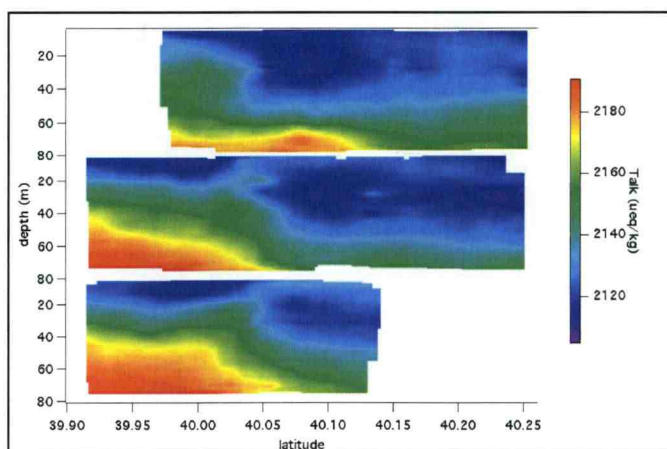


Figure 8. Gridded data for A) measured TCO₂, B) measured PCO₂, and C) calculated alkalinity transects across New England shelfbreak front. SeaSoar track is shown in A) to demonstrate sampling density of Sea Soar. Front transition zone indicated by dotted line in B).

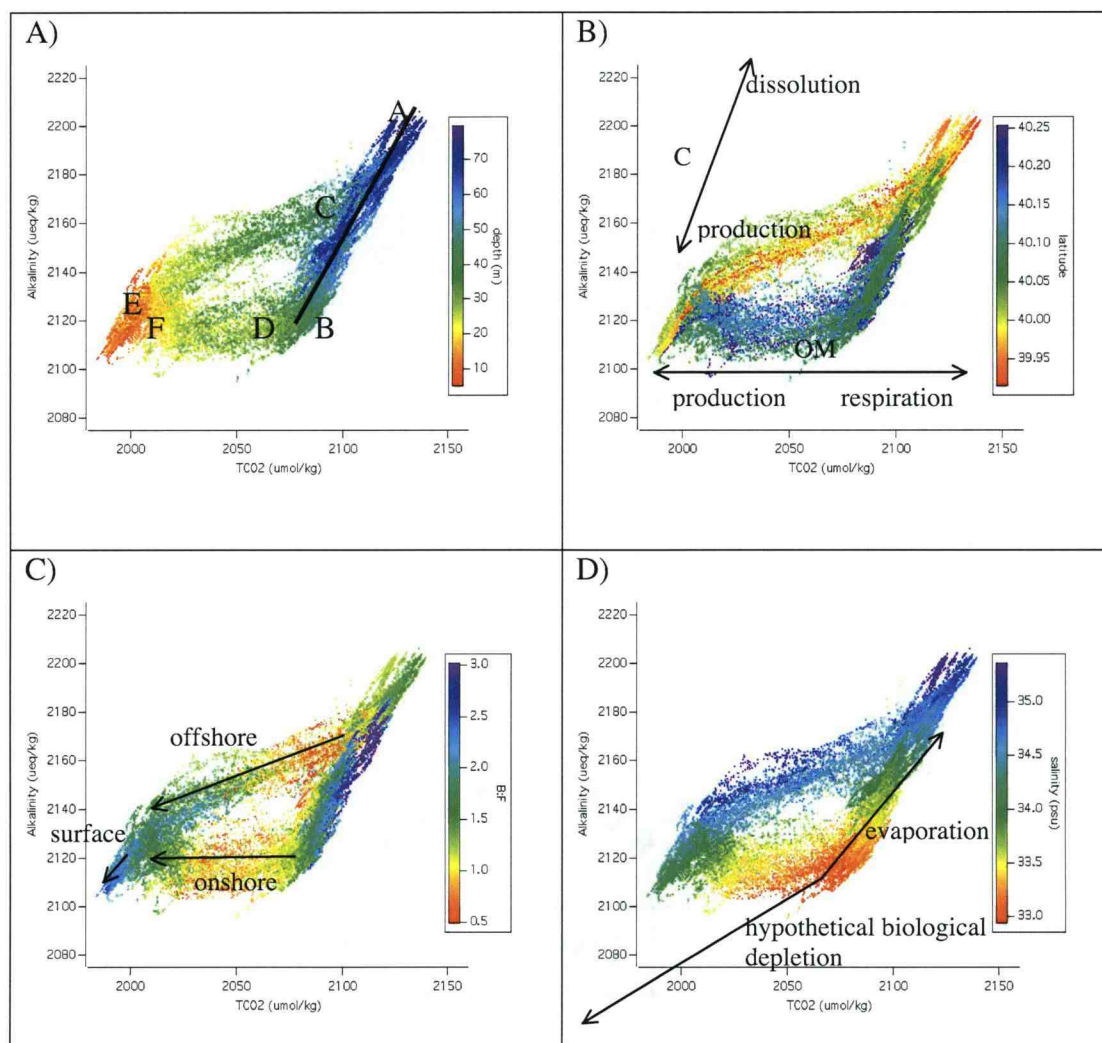


Figure 9. Alkalinity and TCO₂ distributions. A) Symbols are colored as depth of measurements. A is offshore deep water, and B is onshore deep water; these water masses mix conservatively along the line. Points C and D represent the beginning of deviations from conservative mixing offshore and onshore, respectively. Points E and F represent surface waters offshore and onshore of the front, respectively. B) Symbols are colored as latitude. OM arrow shows the effects of net respiration and production on TCO₂ and alkalinity. C arrow shows the effects of calcite production and dissolution. C) Symbols are colored as B:F ratio, which is used as a proxy for calcite producers. D) Symbols are colored as salinity.

corresponding closely with the C arrow. This implies that calcite production can be a dominant process in very near-surface waters on either side of the front.

Additional support for this implied planktonic calcite production comes from *in situ* measurements of optical backscatter and chlorophyll fluorescence. The relationship between backscatter (B, arbitrary units) and particle density is a complicated function of particle size and composition (Balch et al., 1991, 1996a, 1996b), but for our purposes, we will consider backscatter to be a rough proxy for the total particulate matter in the water. Chlorophyll fluorescence (F, arbitrary units) is roughly proportional to the concentration of fluorescing chlorophyll in organisms present in the water. A parcel of water with a high concentration of non-fluorescing, chlorophyll-free particles would thus have a high B:F ratio. If these non-fluorescing particles were calcite shells, we would expect a high B:F ratio to coincide with a high $\Delta\text{alkalinity}:\Delta\text{TCO}_2$ ratio. The colors of the symbols of Figure 9C represent this ratio. Data within the most extreme biogenic departure from the mixing line (points E and F) in surface waters show a high B:F ratio, indicating a high percentage of non-fluorescing material. Offshore mid-depth waters (between points C and E) show a higher B:F ratio than onshore waters (between points D and F), implying that more calcite producers are present in offshore waters. While our analysis is qualitative, it is consistent with the conclusion drawn from the alkalinity and TCO_2 data that calcareous plankton significantly affect the carbonate chemistry of offshore waters.

Estimates of upward vertical nitrate and silicate fluxes in these same sections provide additional support for the importance of planktonic calcite production in offshore waters. Nitrate fluxes at the nutricline show little cross-front variability in these sections, while silicate fluxes decrease dramatically on the seaward side of the front (Covert et al., 2003b). If these nutrient fluxes are driven by net biological consumption in surface waters, the similar onshore and offshore nitrate fluxes imply similar levels of net photosynthetic production on both sides of the front. The decreased silicate fluxes offshore relative to onshore, however, imply a relative decrease in the production of opal-producing plankton such as diatoms, and that some other phytoplankton group is responsible for maintaining the offshore nitrate uptake.

It is likely, based on these nutrient uptake rates, that calcite producers play a more dominant role offshore than onshore and might account for the nitrate uptake offshore in the absence of silicate producers. This is consistent with the canonical idea that coccoliths favor open ocean, blue water conditions (discussed in Balch et al., 1991).

Variations in fresh water inputs or losses can also affect these distributions. Figure 9D again shows the alkalinity and TCO_2 relationship, where the symbols' colors represent the salinity of each data point. Onshore, the salinity increases from 33 to 34 psu, a 3% increase, coincident with decreasing TCO_2 and essentially unchanged alkalinity. One possible explanation for these coincident changes is that surface waters onshore of the front have experienced extensive freshwater loss, either due to evaporation or decreased input of low-salinity river water from the continent. While the input of buoyant fresh water from terrestrial runoff affects the front along the east coast of North America (Chapman et al., 1989; Yankovsky et al., 1997; Chapman, 2003), rivers typically have fairly high concentrations of bicarbonate ion (and thus TCO_2 and alkalinity) despite their near-zero salinity (discussed in numerous textbooks, including Morel and Herring, 1993; Berner and Berner, 1996; and Pilson, 1998). Therefore, a salinity increase due to reduction of input of river water would have much smaller confounding effect on alkalinity and TCO_2 than would evaporative loss of pure water vapor, so we will examine the effects of evaporation here.

An evaporative loss that drives a 3% salinity increase would simply concentrate TCO_2 and alkalinity in the same relative proportion, as shown by the evaporation arrow on Figure 9D. The observed TCO_2 and alkalinity depletions would thus be underestimates of the true biological uptake of these species. We estimate that the evaporation-corrected biogenic alkalinity uptake is about 64 ueq/L, and the evaporation-corrected biogenic TCO_2 uptake is approximately 132 $\mu\text{mol/L}$, shown by the hypothetical biological depletion arrow in Figure 9D. This implies an onshore $\Delta\text{alkalinity}:\Delta\text{TCO}_2$ of about 1 to 2, very close to the offshore ratio of 1 to 3. This suggests that organic matter and calcite production might occur in similar proportions onshore and offshore when corrections for evaporation are made in onshore waters alone. It is likely that evaporation affects offshore surface waters as well; however,

the strongest depletions in offshore alkalinity and TCO_2 relative to deep waters happen at near-constant salinities of about 34.5 psu, and no evaporative correction can be meaningfully applied in such a case.

Finally, mixing of water masses also has the potential to affect the distributions of alkalinity and TCO_2 . We considered several simplified scenarios, including mixing of non-biologically-affected onshore water with biologically-affected offshore water, mixing of non-biologically-affected onshore and offshore waters with a third water mass with characteristics coinciding with the near-intersection of onshore and offshore surface water properties, and mixing of onshore and/or offshore waters with an unknown third water mass in such a way that onshore and offshore waters were allowed to maintain the same biological TCO_2 and alkalinity uptake ratios. Each of these, however, necessitated the existence of water masses with unrealistic properties or the absence of essentially all biological productivity on one or both sides of the front, and we do not present the results of this exercise fully here. There are, of course, more complicated scenarios involving even more unknown water masses and the simultaneous combination of mixing, evaporation, and loss of terrestrial freshwater input that could be applied. Given the data at hand, however, we cannot hope to adequately constrain these, and we do not attempt to.

7. Conclusions

We developed a system to measure the total inorganic carbon concentration of a continuously flowing stream of seawater based on a gas permeable membrane contactor, a non-dispersive infra-red (NDIR) gas analyzer, and invariant gas and liquid flows. This system continuously acidifies the sample stream and quantitatively strips the evolved CO_2 out in the membrane contactor. The CO_2 in the strip gas stream is then analyzed using a NDIR gas analyzer. The system can resolve TCO_2 concentrations to better than $\pm 0.1\%$ and has a response time of 6 seconds.

This system has several advantages over other sea-going TCO_2 analyzers. It is easy to set up, involves short start up times, and requires only small volumes of 10% HCl as the reagent. In addition, the system continuously analyzes the TCO_2

concentration of a flowing stream without subsampling the seawater stream.

Coupled with the Lamont Pumping SeaSoar system, this TCO_2 analyzer has allowed us to collect the first high resolution TCO_2 data of its kind. In conjunction with simultaneously-measured PCO_2 data, we were able to calculate high-resolution distributions of alkalinity, another first.

Based on cross-front depletions of alkalinity and TCO_2 , we identified the effects of biogenic calcite production, and concluded that calcite producers play a dominant role offshore of the New England shelfbreak front. This is supported by optical measurements indicating a higher percentage of non-fluorescing material in offshore waters than in onshore waters, with the highest percentage of non-fluorescing material in surface water; by cross-front distributions of nitrate and silicate vertical fluxes, which suggest a dramatic decrease in silicate-consuming plankton seaward of the front; and by the canonical notion that coccolithophores are favored in warmer, open ocean waters (as discussed in Balch et al., 1991). Although an extreme correction for the effects of evaporation, applied only to waters shoreward of the front, allows organic matter and calcite production to occur at the same ratio across the front, we feel that the most consistent interpretation of all the data is one with increasing biogenic calcite production, and decreasing biogenic opal production, in the warmer, clearer offshore waters. We believe that this is the first time that the activities of calcite producers in surface waters have been diagnosed by alkalinity depletions.

III. CONCLUSION

The flow-through TCO_2 analyzer allows for the collection of high-resolution TCO_2 data with high precision and high internal accuracy. These data, coupled with high-resolution PCO_2 and CTD data, provide sufficient information to fully constrain the carbonate system, allowing for the calculation of alkalinity, pH, and HCO_3^- and CO_3^{2-} concentrations.

This analytical system will benefit from improved at-sea standardization techniques. Some techniques have been tried but not yet rigorously tested in the laboratory. To further reduce gas exchange, the liquid standards can be stored in gas-impermeable bags which collapse as the standards are used, eliminating concern about exchange with a changing headspace.

The TCO_2 system has been deployed on 4 cruises: the Southern Ocean Iron Experiment (SOFEX) cruise in the Southern Ocean in January 2002, the New England Shelfbreak Productivity Experiment (NESPEX) cruises 2 and 3 at the New England shelfbreak front in June and August 2002, and the Coastal Ocean Advances in Shelf Transport (COAST) cruise 3 off the Oregon coast in January 2003. Although the system was still in the testing phase for the SOFEX cruise, reliable data was collected and used to examine general C:N ratios in and outside of the fertilized patch (Coale et al., 2004). In the future, we hope to examine these data more specifically to study differences between the northern and southern fertilization patches and across patch boundaries.

High-resolution PCO_2 data and discrete TCO_2 samples (collected before the TCO_2 system was operational) analyzed in the laboratory have allowed us to roughly calculate the preformed nutrient concentrations of water upwelled at the Oregon coast and determine that this region acts as a sink for CO_2 (Hales, Takahashi, Bandstra, submitted).

High-resolution physical measurements were collected on the COAST 3 and NESPEX 2 and 3 cruises. Preliminary work with data from COAST cruises 1 and 2 has shown that, by combining the highly variable physical mixing data with the highly variable nutrient gradient data, we can calculate more precise values for turbulent

mixing across isopycnals than have been possible with coarsely-resolved chemical measurements and approximations of mixing coefficients (Covert et al., 2003b). In the future, we will perform similar calculations with carbonate data to estimate biological rates of production and calcite formation. These kinds of measurements and calculations will allow researchers to better quantify important rates and processes affecting biogeochemical cycles in the ocean.

BIBLIOGRAPHY

- Balch, W.M., Holligan, P.M., Ackleson, S.G., Voss, K.J., 1991. Biological and optical properties of mesoscale coccolithophore blooms in the Gulf of Maine. *Limn. Oceanog.*, 36(4), 629-643.
- Balch, W.M., Kilpatrick, K.A., Trees, C.C., 1996a. The 1991 coccolithophore bloom in the central North Atlantic. 1. Optical properties and factors affecting their distribution. *Limn. Oceanog.*, 41(8), 1669-1683.
- Balch, W.M., Kilpatrick, K.A., Holligan, P., Harbour, D., Fernandez, E., 1996b. The 1991 coccolithophore bloom in the central North Atlantic. 1. Relating optics to coccolith concentration. *Limn. Oceanog.*, 41(8), 1684-1696.
- Berner, E.K., Berner, R.A., 1996. Global environment: water, air, and geochemical cycles. Prentice-Hall, Inc., New Jersey.
- Broecker, W.S., Takahashi, T., 1966. Calcium carbonate precipitation on the Bahama Banks. *JGR*, 71, 1575-1602.
- Chapman, D.C., Beardsley, R.C., 1989. On the origin of shelf water in the middle Atlantic bight. *J. Phys. Oceanog.*, 19, 384-391.
- Chapman, D.C., 2003. Separation of an advectively trapped buoyancy current at a bathymetric bend. *J. Phys. Oceanog.*, 33, 1108-1121.
- Coale, K.H., Johnson, K.S., Chavez, F.P., Buesseler, K.O., Barber, R.T., Brzezinski, M.A., Cochlan, W.P., Wanninkhof, R.H., Kudela, R.M., Altabet, M.A., Hales, B.R., Takahashi, T., Landry, M.R., Bidigare, R.R., Wang, X., Chase, Z., Strutton, P.G., Friederich, G.E., Gorbunov, M.Y., Lance, V.P., Hilting, A.K., Hiscock, M.R., Demarest, M., Hiscock, W.T., Sullivan, K.F., Tanner, S.J., Gordon, R.M., Hunter, C.N., Elrod, V.A., Fitzwater, S.E., Jones, J.L., Tozzi, S., Koblizek, M., Roberts, A.E., Herndon, J., Brewster, J., Ladizinsky, N., Smith, G., Cooper, D., Timothy, D., Brown, S.L., Selph, K.E., Shelidan, C.C., Twining, B.S., Johnson, Z.I., 2004. Southern Ocean Iron Enrichment Experiment: carbon cycling in high- and low-silicate waters. *Science*, 304, 408-414.
- Covert, P., Hales, B., Hebert, D., Houghton, R., 2003a. Vertical fluxes of nitrate and silicate at the New England shelf-break front: implications for distribution of diatom productivity. *EOS Trans. AGU*, 84(52), Ocean Sci. Meet. Suppl., Abstract OS52H-03.
- Covert, P., Hales, B., Moum, J., Jennings, J., Bandstra, L. 2003b. Vertical fluxes of nitrate on the Oregon shelf based on co-incident high-resolution measurements of

nitrate gradients and turbulent mixing rates. EOS Trans. AGU, 84(52), Ocean Sci. Meet. Suppl., Abstract OS42M-06.

Dickson, A.G., 1984. pH Scales and proton-transfer reaction in saline media such as seawater. *Geo. Cosmo. Acta.*, 48, 2299-2308.

Dickson, A.G., 1993a. pH buffers for sea water based on the total hydrogen ion concentration scale. *Deep-Sea Res.*, 40, 107-118.

Dickson, A.G., 1993b. The measurement of sea water pH. *Mar. Chem.*, 44, 131-142.

Dickson, A.G. and Goyet, C. (Editors), 1994. DOE Handbook of methods for the analysis of the various parameters of carbon dioxide system in seawater, Version 2, ORNL/CDIAC-74.

Dyrssen, D., Sillen, L.G., 1967. Alkalinity and total carbonate in sea water: a plea for P-T-independent data. *Tellus*, 19, 113-121.

Goyet, C., Snover, A.K., 1993. High-accuracy measurements of total dissolved inorganic carbon in the ocean: comparison of alternative detection methods. *Mar. Chem.* 44, 235-242.

Hales, B., Takahashi, T., 2002. The pumping SeaSoar: a high-resolution seawater sampling platform. *J. Atm. and Oceanic Tech.* 19, 1096-1104.

Hales, B., Chipman, D., Takahashi, T., 2004. High-frequency measurement of partial pressure and total concentration of carbon dioxide in seawater using microporous hydrophobic membrane contactors. *Limn. And Oceanog. Methods*, in press.

Hales, B., Takahashi, T., 2004. High-resolution biogeochemical investigation of the Ross Sea, Antarctica, during AESOPS (U.S. JGOFS) program. *JGR*, in press.

Hales, B., Takahashi, T., Bandstra, L., submitted. Atmospheric CO₂ uptake by a coastal upwelling system.

Hales, B. Supersucker methods, in prep.

Johnson, K.M., King, A.E., Sieburth, J.M., 1985. Coulometric TCO₂ analyses for marine studies: an introduction. *Mar. Chem.*, 16, 61-82.

Johnson, K.M., Sieburth, J.M., Williams, P.J.leB., Brandstrom, L., 1987. Coulometric TCO₂ analyses for marine studies: automation and calibration. *Mar. Chem.*, 21, 117-133.

- Johnson, K.M., Wills, K.D., Butler, D.B., Johnson, W.K., Wong, C.S., 1993. Coulometric TCO₂ analyses for marine studies: maximizing the performance of an automated gas extraction system and coulometric detector. *Mar. Chem.*, 44, 167-187.
- Keeling, C.D., Whorf, T.P., 2004. Atmospheric CO₂ records from sites in the SIO air sampling network. In *Trends: A Compendium of Data on Global Change*. Carbon Dioxide Information Analysis Center, Oak ridge National Laboratory, U.S. Department of Energy, Oak Ridge, Tenn., U.S.A.
- Kanomori, S., 1982. Shipboard calibration of an infrared absorption gas analyzer. *J. Ocean. Soc. Japan.*, 38, 131-136.
- Kimoto, H., Nozaki, K., Kudo, S., Kato, K., Negishi, A., Kayanne, H., 2002. Achieving high time-resolution with a new flow-through type analyzer for total inorganic carbon in seawater. *Japan Soc. Anal. Chem.*, 18, 247-255.
- Lamb, M.F., Sabine, C.L., Feely, R.A., Wanninkhof, R., Key, R.M., Johnson, G.C., Millero, F.J., Lee, K., Peng, T.-H., Kozyr, A., Bullister, J.L., Greely, D., Byrne, R.H., Chipman, D.W., Dickson, A.G., Goyet, C., Guenther, P.R., Ishii, M., Johnson, K.M., Keeling, C.D., Ono, T., Shitashima, K., Tilbrook, B., Takahashi, T., Wallace, D.W.R., Watanabe, Y.W., Winn, C., Wong, C.S., 2002. Consistency and synthesis of Pacific Ocean CO₂ survey data. *Deep-Sea Res. II*, 49, 21-58.
- Martin, J.H., 1990. Glacial-interglacial CO₂ change: the iron hypothesis. *Paleoceanography*, 5, 1-13.
- Millero, F.J., 1995. Thermodynamics of the carbon dioxide system in the oceans. *Geo. Cosmo. Acta.*, 59, 661-667.
- Morel, F.M.M, Herring, J.G, 1993. Principles and applications of aquatic chemistry. John Wiley & Sons, Inc, New York.
- O'Sullivan, D.W. and Millero, F.J., 1998. Continual measurement of the total inorganic carbon in surface seawater. *Mar. Chem.*, 60, 75-83.
- Park, K., Kennedy, G.H., Dobson, H.H., 1964. Comparison of gas chromatography method and pH-alkalinity method for determination of total carbon dioxide in sea water. *Anal. Chem.*, 36, 1686.
- Park, P.K., 1969. Oceanic CO₂ system: an evaluation of ten methods of investigation. *Limnol. Oceanog.*, 14, 179-186.
- Petit, J.R., Raynaud, D., Barkov, N.I., Barnola, J.-M., Basile, I., Bender, M., Chappellaz, J., Davis, M., Delaygue, G., Delmotte, M., Kotlyakov, V.M., Legrand, M., Lipenkov, V.Y., Lorius, C., Pepin, L., Ritz, C., Saltzman, E., Stievenard, M.,

1999. Climate and atmospheric history of the past 420,000 years from the Vostok ice core, Antarctica. *Nature*, 399, 6735, 429-436.

Pilson, M.E.Q., 1998. *An Introduction to the chemistry of the sea*. Prentice Hall, New Jersey.

Pytkowicz, R.M., Kester, D.R., and Burgener, B.C., 1966. Reproducibility of pH measurements in seawater. *Limnol. Oceanog.*, 11, 417-419.

Weiss, R.F., Craig, H., 1973. Precise shipboard determination of dissolved nitrogen, oxygen, argon, and total inorganic carbon by gas chromatography. *Deep-Sea Res.*, 20, 291-303.

Wong, C.S., 1970. Quantitative analysis of total carbon dioxide in sea water: a new extraction method. *Deep-Sea Res.*, 17, 9-17.

Yankovsky, A.E., Chapman, D.C., 1997. A simple theory for the fate of buoyant coastal discharges. *J. Phys. Oceanog.*, 27, 1386-1401.

APPENDICES

Appendix A. Artificial seawater recipe and the carbon content of NaHCO_3 and salts.

Table A1. Artificial seawater recipe.

salt	g salt/L distilled water
NaCl	25
CaCl_2	1
Na_2SO_4	4
$\text{MgCl}_2 \cdot 6\text{H}_2\text{O}$	10.7

Table A2. Carbon content of cystine standards. Analyses was performed on a Carlo-Erba NA150. The carbon content of the standards was 29.99%.

standard #	CO_2	CO_2 -blank	sample wt	mg CO_2
1	1,926,572	1,921,663	1.0243	0.3072
2	1,004,500	999,591	0.5279	0.1583
3	1,999,643	1,994,734	1.0516	0.3154
4	2,278,572	2,273,663	1.2066	0.3619
5	1,287,827	1,282,918	0.6749	0.2024
6	1,558,729	1,553,820	0.8196	0.2458
7	783,574	778,665	0.4117	0.1235
8	1,372,209	1,367,300	0.7201	0.2160
9	334,725	329,816	0.1752	0.0525
10	1,225,043	1,220,134	0.6441	0.1932
11	1,525,383	1,520,474	0.8022	0.2406
12	1,724,730	1,719,821	0.9176	0.2752
blank	4,909	0		

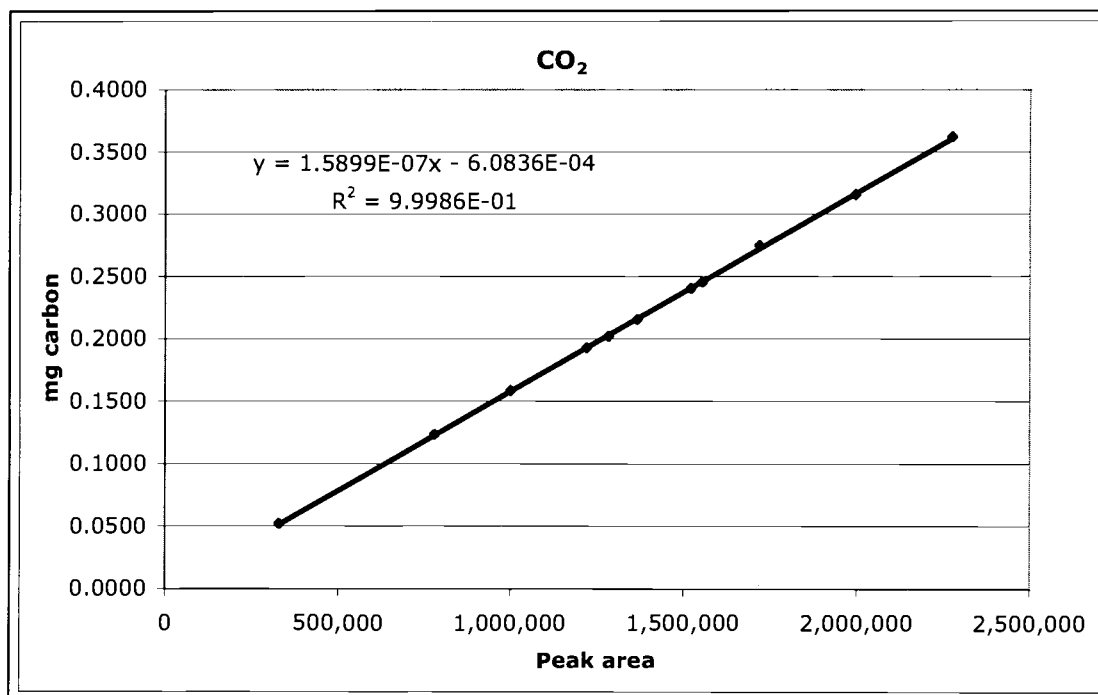


Figure A1. Calibration curve of cystine standards using blank-corrected values.

Table A3. Carbon content of NaHCO₃ used to prepare standards for TCO₂ analyses. The average carbon content of the NaHCO₃ was 14.43%. This value is 0.93% higher than the value expected based on formula weight, 14.29%.

NaHCO ₃ sample	CO ₂	CO ₂ -blank	sample wt	mg CO ₂	mg C/mg NaHCO ₃
1	1,380,693	1,375,784	1.5098	0.2173	0.1440
2	1,755,106	1,750,197	1.9282	0.2769	0.1436
3	1,501,293	1,496,384	1.6532	0.2365	0.1431
4	1,630,021	1,625,112	1.7871	0.2570	0.1438
5	1,089,446	1,084,537	1.1927	0.1710	0.1434
6	1,979,146	1,974,237	2.1716	0.3125	0.1439
7	790,390	785,481	0.8642	0.1235	0.1429
8	1,488,054	1,483,145	1.6406	0.2344	0.1429
9	1,746,146	1,741,237	1.91	0.2755	0.1442
10	1,532,897	1,527,988	1.6794	0.2415	0.1438
11	1,007,110	1,002,201	1.0946	0.1580	0.1443
12	1,542,986	1,538,077	1.6884	0.2432	0.1440
13	1,628,616	1,623,707	1.778	0.2568	0.1444
14	880,784	875,875	0.9544	0.1379	0.1445
Blank	4,909	0			

Table A4. Carbon content of salts used to prepare artificial seawater. Duplicate analyses were performed for each salt.

salt sample	mg C/mg salt
NaCl	1.046E-05
CaCl ₂	-1.5335E-05
Na ₂ SO ₄	4.16733E-08
MgCl ₂ .6H ₂ O	-1.72953E-05

Appendix B. Membrane contactor stripping efficiency test.

Table B1. Data for range of $F_G:F_L$ and the associated stripping efficiencies.

$TCO_{2,in}$ ($\mu\text{mol/mL}$)	F_G (mL/min)	F_L (mL/min)	$XCO_{2,out}$ ($\mu\text{mol/mol}$)	$F_G:F_L$	Stripping Efficiency @ 273K
2.02	1000	19.94	806.03	50.146	0.893
2.02	950	19.94	846.48	47.639	0.891
2.02	900	19.94	892.72	45.132	0.890
2.02	850	19.94	942.46	42.624	0.887
2.02	800	19.94	994.52	40.117	0.881
2.02	750	19.94	1055.52	37.610	0.877
2.02	700	19.94	1119.92	35.102	0.868
2.02	650	19.94	1202.80	32.595	0.866
2.02	600	19.94	1284.17	30.088	0.854
2.02	550	19.94	1385.72	27.580	0.844
2.02	500	19.94	1502.10	25.073	0.832
2.02	400	19.94	1836.33	20.059	0.814
2.02	300	19.94	2357.89	15.044	0.784

These data are plotted in Figure 2 of Chapter II. Stripping efficiency, E , is calculated as follows:

$$E = \frac{F_G}{F_L} \frac{\gamma XCO_{2,out}}{TCO_{2,in}}$$

At 273 K, γ is equal to 4.46×10^{-5} mol gas/mL gas (or the inverse of 22,410 mL/mol gas).

Appendix C. Response time test and first-order model.

Table C1. XCO₂ change after step function change in input signal.

XCO ₂ (μmol/mol)
1097.9
1098.7
1099.4
1100
1100.3
1100.5
1102
1105.2
1108.4
1118.9
1131.2
1141.4
1149.7
1156.5
1161.2
1162.9
1164.1
1166.7
1168.8
1169.1
1168.8
1170.3
1171.4
1170.5
1170.6
1171.1
1170.3
1170.6
1171.5
1171.8
1171.8

The data in Table C1 were modeled using a simple first order exponential rise equation to estimate the response time of the system, τ :

$$C(t) = C_o + (C_f - C_o)(1 - e^{-t/\tau})$$

where C_o is the initial value before the step function increase, C_f is the final value, and τ is the response time of the system. The following values were used:

$$C_o = 1100$$

$$C_f = 1171.$$

From this model, τ was calculated to be 6 seconds.

Table C2. Model data fit to step function rise data. This model was used to estimate the response time, τ , of the system. The model and data are shown in Figure 3 of Chapter II.

Model XCO ₂
1100
1120.12628
1134.54738
1144.88056
1152.2846
1157.58983
1161.39119
1164.11499
1166.06667
1167.46512
1168.46715
1169.18513
1169.69959
1170.06822
1170.33235
1170.52161
1170.65722
1170.75438
1170.82401
1170.8739
1170.90964
1170.93526
1170.95361

Appendix D. Stability and precision of TCO₂ system.Table D1. Long-term stability of TCO₂ system.

	Detector response
before standards	2286.03
between standards	2287.15
after standards	2283.66

Table D2. Concentrations of TCO₂ standards (TCO₂) and LI-COR output (XCO₂).

Standard #	TCO ₂ (μmol/kg)	XCO ₂ (μmol/mol)
1	1934.51	829.5
2	1987.27	851.7
3	2021.98	866.3
4	2092.84	895.77
blank	0	8.77

The XCO₂ for the blank was multiplied by the slope of the calibration curve obtained by linear regression of the above data. That TCO₂ blank, representing the TCO₂ of the artificial seawater in μmol/kg, was added to the TCO₂ values in the above table, as shown in Table D3.

Table D3. Blank-corrected TCO₂ values and the deviations. The linear regression is shown in Figure 5 of Chapter II. The average of the deviations from the linear regression is 0.009%.

Standard #	XCO ₂ (μmol/mol)	Blank-corrected TCO ₂ (μmol/kg)	Calculated TCO ₂ (μmol/kg)	Deviation from linear regression
1	829.5	1955.466	1955.2735	0.010%
2	851.7	2008.222	2008.31374	0.005%
3	866.3	2042.934	2043.19606	0.013%
4	895.8	2113.796	2113.605784	0.009%
blank	8.77	20.953		

An independent check sample was run with the standards and its TCO₂ concentration was analyzed based on the standard curve.

Table D4. Independent check sample value.

	Prepared TCO ₂ (μmol/kg)	XCO ₂ (μmol/mol)	Calculated TCO ₂ (μmol/kg)	Deviation from prepared value
independent check sample	1986.84	852.8	1989.99	0.159%

Appendix E. Accuracy check samples.

Table E1. Coulometrically-analyzed check samples. They are compared to data from continuously-flowing TCO₂ system as shown in Figure 6 of Chapter II. The average of the differences between the check sample values and the TCO₂ system values is 0.08%.

Time of Check Sample (decimal day)	Check Sample Value ($\mu\text{mol/kg}$)	TCO ₂ System Value ($\mu\text{mol/kg}$)	Deviation from Check Sample
223.7863773	2000.73	1999.66	0.05%
223.7870718	2063.9	2061.3	0.13%
223.7877662	2073.75	2075.3	0.07%

Appendix F: Analyses of certified reference materials, Batch 63.

Table F1. Our analyses of CRM batch 63 samples. These data were collected using the TCO₂ analysis system described in this work.

Bottle #	Calibrated TCO ₂ (μmol/kg) from this work
88	2011.47
88	2011.33
55	2010.38
55	2013.47
317	2016.34
584	2013.18
621	2013.89
450	2014.57
584	2015.51
621	2013.62
450	2016.83

The average TCO₂ value for Batch 63 samples based on this work was 2013.69 ± 2.07 μmol/kg.

Table F2. LDEO analyses of CRM batch 63 samples. These data were collected coulometrically.

Bottle #	Calibrated TCO ₂ (μmol/kg) from LDEO
517	2013.6
517	2013.9
517	2015.7
217	2015.0
217	2013.1
217	2013.4

The average TCO₂ value for Batch 63 samples based on LDEO measurements was 2014.1 ± 1.01 μmol/kg.

Appendix G. Alkalinity calculations from TCO_2 and PCO_2 .

Total alkalinity can be calculated given the following definitions and acid-base equilibrium relationships:

$$\text{TCO}_2 = [\text{HCO}_3^-] + [\text{CO}_3^{2-}] + [\text{CO}_{2(aq)}]$$

$$\text{PCO}_2 = \frac{[\text{CO}_{2(aq)}]}{K_H}$$

$$K_1 = \frac{[\text{HCO}_3^-]\{\text{H}^+\}}{[\text{CO}_{2(aq)}]}$$

$$K_2 = \frac{[\text{CO}_3^{2-}]\{\text{H}^+\}}{[\text{HCO}_3^-]}.$$

The constants K_H , K_1 , and K_2 are temperature- and salinity- dependent as well, and we have used the equations in Pilson (1998) for these calculations. For our purposes, we have defined alkalinity as:

$$\text{total alkalinity} = [\text{HCO}_3^-] + 2[\text{CO}_3^{2-}] + [\text{B(OH)}_4^-].$$

There are several other acid-base reactive species that can contribute to the total alkalinity, including phosphate, silicate, and organic acids, but the conjugate bases of carbonic and boric acids are the most important. The concentration of borate, $[\text{B(OH)}_4^-]$ can be estimated by :

$$\text{B(OH)}_4^- = \frac{[\text{TB}]K_B}{K_B + \{\text{H}^+\}}$$

where $[\text{TB}]$ is total borate, which is approximately conservative with salinity by the following relationship:

$$[\text{TB}] = \frac{0.426}{35} S$$

and K_B is the temperature- and salinity- dependent dissociation constant of boric acid as given in Pilson (1998).

Rearrangement and combination of the above equations leads to the following equation for TCO_2 :

$$TCO_2 = \frac{K_2}{K_1 CO_{2(aq)}} [HCO_3^-]^2 + [HCO_3^-] + [CO_{2(aq)}].$$

Since TCO_2 and PCO_2 are measured, HCO_3^- is the only unknown in this equation, which can be solved for HCO_3^- . HCO_3^- can then be substituted into the following equation to get CO_3^{2-} :

$$CO_3^{2-} = \frac{K_2 HCO_3^-}{H^+}.$$

The values for $[CO_3^{2-}]$ and $[HCO_3^-]$ can then be substituted into the alkalinity equation along with the calculated $[B(OH)_4^-]$ to calculate total alkalinity from the measured TCO_2 and PCO_2 values.